Multiport Power Divider–Combiner Circuits Using Circular-Sector-Shaped Planar Components

MOHAMED D. ABOUZAHRA, SENIOR MEMBER, IEEE, AND KULDIP C. GUPTA, FELLOW, IEEE

Abstract—**A novel sector-shaped circuit configuration is proposed for designing planar power dividers–combiners that are compatible with microstrip circuits. This configuration is analyzed by using the two-dimensional planar circuit approach. Expressions for impedance matrix parameters of multiport sectorial planar circuits are given. Theoretical and experimental results reported for 90° and 180° power dividers are in good agreement.**

I. INTRODUCTION

MASSIVE POWER divider and power combiner circuits are used extensively at microwave and millimeter-wave frequencies. When these circuits are needed in planar (microstrip-type) configurations, two particular circuit types are often used. These are the symmetric geometry with radially oriented lines [1]–[2] and the fan-out, Wilkinson-type geometry [3]. The use of circular disk planar segments for designing symmetrical power combiner–divider circuits has been discussed in a recent paper [4]. The present paper reports the use of the sector-shaped planar segments for designing power divider–combiner circuits.

One system application that motivated this investigation is the need for replacing the lossy corporate feed structures used in feeding a linear array of antenna elements. A circular disk geometry with output lines extending radially in all directions is not appropriate for this purpose. On the other hand, a sector geometry with almost linearly aligned output ports (Fig. 1) is topologically more suitable. Also, the sector geometry shown in Fig. 1 is truly planar as there is no need for the vertically oriented feed port which is used in the circularly symmetric configuration [4]. This, of course, makes it easy to integrate these circuits in the same plane and on both the input and output sides. Furthermore, these power divider–combiner circuits could be cascaded in a fan-out or a fan-in manner as shown in Fig. 2. Another promising feature offered by these circuits is the flexibility in obtaining unequal output power levels at various ports. This characteristic can be used for the amplitude tapering feature often required in antenna arrays. The power level at the various output ports (Fig. 1) can be controlled by adjusting the locations and/or widths of the microstrip lines connected to these ports. Altering the widths of the output ports, however, may require the inclusion of quarter-wave impedance transformers so that proper match can be ensured.

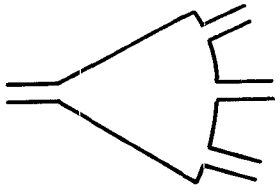

Fig. 1. Geometry of a sectorial power divider/combiner circuit.

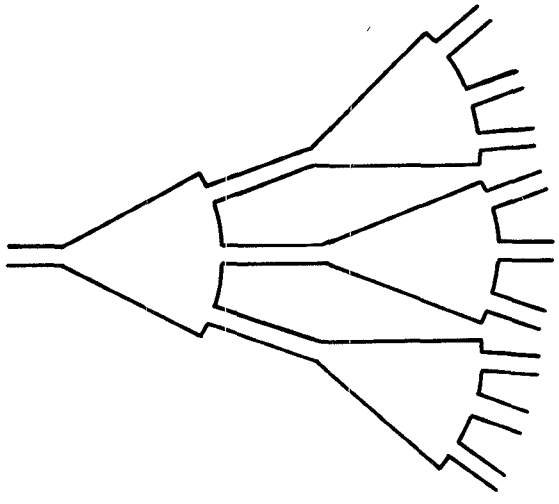

Fig. 2. Cascading of sectorial power divider/combiner circuits.

This paper describes the analysis of these circuits by the two-dimensional planar circuit approach [5]. The impedance matrix elements for sector-shaped segments have been derived and are given in the next section. Four-way and five-way power divider circuits have been designed, fabricated, and tested. The measured and calculated scattering parameters are found to be in good agreement.

Manuscript received April 13, 1988; revised August 25, 1988. This work was supported in part by the Department of the Air Force

M. D. Abouzahra is with the MIT Lincoln Laboratory, Lexington, MA 02173.

K. C. Gupta is with the Department of Electrical and Computer Engineering, University of Colorado, Boulder, CO 80309.

IEEE Log Number 8824340.

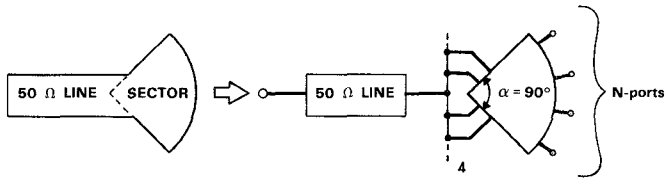

Fig. 3. Modeling procedure of the 90° sectorial circuits.

II. Theoretical Analysis

The planar circuit analysis approach previously used [4] for circular disk power divider circuits is also applicable to circuits with sectorial geometry. The analysis procedure for 90° and 180° sectorial circuits is summarized in this section.

A. Analysis of 90° Sectorial Circuit

The analysis of the 90° circular sector sketched in Fig. 3 is carried out by deriving the Z-matrix elements using [5]

$$Z_{ij} = \frac{1}{W_i W_j} \int_{W_i} \int_{W_j} G(s_i/s_j)\, ds_i\, ds_j \tag{1}$$

where W_i and W_j, respectively, represent the effective widths [5] of ports i and j, and ds_i, ds_j are incremental distances along the port widths. The quantity $G(s_i/s_j)$ in (1) denotes the two-dimensional impedance Green's function for the circular sector. The impedance Green's function for a circular sector having a sector angle α equal to integral submultiples of π radians (180°) (i.e., $\alpha = 180°$, 90°, 60°, 45°, 30°, 22.5°, etc.) is available in the literature [5] and is used here for deriving the impedance matrix. Upon substituting $G(s_i/s_j)$ into (1) and carrying out the integrations, various elements of the impedance matrix are obtained.

When the ports are located along the curved edge (see Fig. 4) of the sector (i.e., at $\rho = a$), the self- and transfer impedance elements of the Z matrix are given by

$$Z_{ij} = \frac{2j\omega\mu d a^2}{\alpha W_i W_j} \cdot \sum_{n=0}^{\infty} \sum_{m=1}^{\infty} \frac{\sigma_n \left\{ \cos(n_s \phi_{ij}) + \cos\left[n_s(\phi_i + \phi_j)\right] \right\}}{n_s^2 \left[a^2 - \frac{n_s^2}{k_{mn_s}^2} \right] \left[k_{mn_s}^2 - k^2 \right]} \cdot \left\{ \cos\left[\frac{n_s}{2}(\Delta_i - \Delta_j)\right] - \cos\left[\frac{n_s}{2}(\Delta_i + \Delta_j)\right] \right\} \tag{2}$$

where the parameter σ_n is defined as

$$\sigma_n = \begin{cases} 1 & \text{for } n = 0 \\ 2 & \text{otherwise} \end{cases} \tag{3}$$

and where $k = k_0\sqrt{\epsilon_r}$. Here ϵ_r is the dielectric constant of the substrate, μ is the permeability, ω is the radial frequency, k_0 is the free-space wavenumber, d is the height of the substrate, α is the sector angle (90° in this case), a is the effective radius of the sector [6], and $W_{i,j}$ are the effective widths of the ports measured along the sector edge $\rho = a$. In addition, the term ϕ_i represents the angular location of port i, $\Delta_i = W_i/a$ is the angular width of port i, ϕ_{ij} is the angular distance between ports i and j, and $n_s = n\pi/\alpha$. The values of k_{mn_s} are determined by the magnetic wall boundary condition at $\rho = a$ and are given by

$$\left. \frac{\partial J_{n_s}(k_{mn_s}\rho)}{\partial \rho} \right|_{\rho = a} = 0. \tag{4}$$

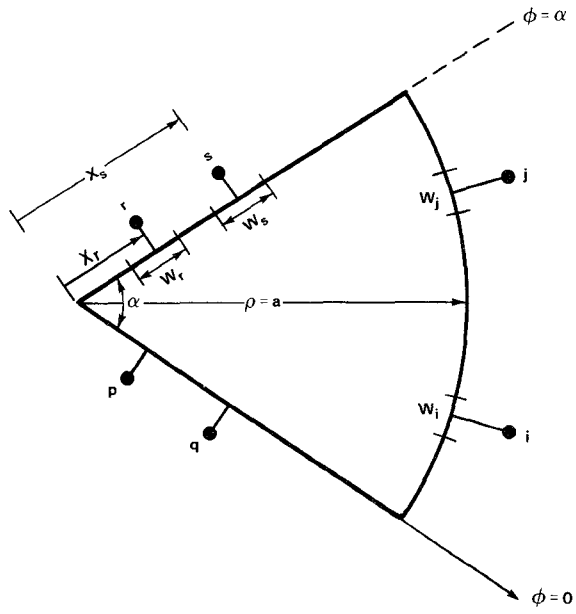

Fig. 4. Port locations and nomenclature of a circular sectorial segment.

When the ports are located along the straight edge $\phi = \alpha$ of the sector, the self- and transfer impedance elements are given by

$$Z_{rs} = \frac{2j\omega\mu d}{\alpha W_r W_s} \cdot \sum_{n=0}^{\infty} \sum_{m=1}^{\infty} \frac{\sigma_n T(\alpha) I_{n_s}(r) I_{n_s}(s)}{\left(k_{mn_s}^2 a^2 - n_s^2\right)\left(k_{mn_s}^2 - k^2\right) J_{n_s}^2(k_{mn_s} a)} \tag{5}$$

where W_r and W_s represent the effective linear widths of the ports and

$$T(\alpha) = \cos^2(n_s \alpha) = 1. \tag{6}$$

In addition,

$$I_{n_s}(r) = \begin{cases} \displaystyle\int_{\gamma_{r1}}^{\gamma_{r2}} J_0(t)\, dt - 2 \sum_{k=0}^{n_s/2-1} \left[J_{2k+1}(\gamma_{r2}) - J_{2k+1}(\gamma_{r1}) \right] \\ \qquad \text{for } n_s \text{ even} \\ J_0(\gamma_{r1}) - J_0(\gamma_{r2}) + 2 \displaystyle\sum_{k=1}^{(n_s-1)/2} \left[J_{2k}(\gamma_{r2}) - J_{2k}(\gamma_{r1}) \right] \\ \qquad \text{for } n_s \text{ odd} \end{cases} \tag{7}$$

with

$$\gamma_{r1} = k_{mn_s}\left(x_r - \frac{W_r}{2}\right) \tag{8}$$

$$\gamma_{r2} = k_{mn_s}\left(x_r + \frac{W_r}{2}\right) \tag{9}$$

where x_r and W_r denote, respectively, the location and the effective width of the port r, as defined in Fig. 4. The term $I_{n_s}(s)$ in (5) is obtained by replacing r with s in (7), (8), and (9).

When the ports are located at the straight edge $\phi = 0$, Z_{pq} is given by (5) with $\alpha = 0$ in (6). Similarly, when one port is located at $\phi = 0$ and the other port is located at $\phi = \alpha$, the transfer impedance element Z_{pr} is also given by (5), but with $T(\alpha) = \cos(n_s\alpha)$ instead.

The transfer impedance element Z_{ir} between two ports, one located at the curved edge $\rho = a$ and the other located at the straight edge $\phi = \alpha$, of the sector is given by

$$Z_{ir} = \frac{4j\omega\mu da}{\alpha W_i W_r} \cdot \sum_{n=0}^{\infty}\sum_{m=1}^{\infty} \frac{\sigma_n \cos(n_s\alpha)\cos(n_s\phi_i)\sin\left(n_s\frac{\Delta_i}{2}\right) I_{n_s}(r)}{n_s k_{mn_s}\left(a^2 - \frac{n_s^2}{k_{mn_s}^2}\right)\left(k_{mn_s}^2 - k^2\right) J_{n_s}(k_{mn_s}a)}. \tag{10}$$

The transfer impedance Z_{ip} between two ports, one located at $\rho = a$ and the other located at $\rho = x_p$ and $\phi = 0$, can be obtained from (10) by setting $\alpha = 0$ in the $\cos(n_s\alpha)$ term.

Upon utilizing (2) through (10), an impedance matrix of dimensions $(N+4)\times(N+4)$ suitable for characterizing the configuration of Fig. 3 is obtained. The term N here represents the number of output ports at the circumference, whereas the number of subports used to model the junction at the feed port is 4. The division of the feed port into several subports (four in this case) accounts for the variation of the edge voltage near the sector apex. The number of subports is chosen such that a constant voltage along the width of each subport is ensured, as required by (1). These four subports, each of width $W_i/4$, are then connected to the feeding microstrip line, and the $(N+4)\times(N+4)$ impedance matrix is reduced to an $(N\times N)$ matrix. This is performed by first converting the $(N+4)\times(N+4)$ Z matrix into the corresponding admittance matrix and then combining the four rows and four columns corresponding to these subports into a single row and a single column as discussed in [5]. The resulting $(N\times N)$ admittance matrix is then converted into a scattering matrix.

Figs. 5 and 6 illustrate, respectively, the calculated scalar S parameters for 90° four-way and five-way power dividers. These figures also include the experimental results discussed later in Section III. In the course of computing these results the values of m and n in the summations

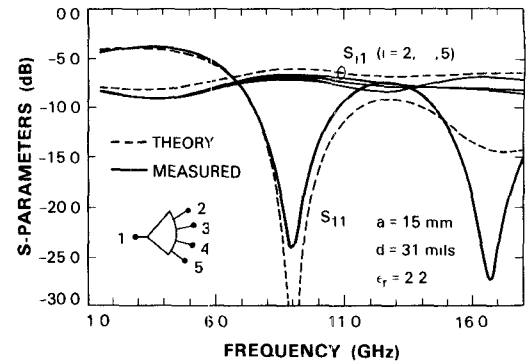

Fig. 5. Measured and calculated scattering parameters of a four-way 90° sector power divider.

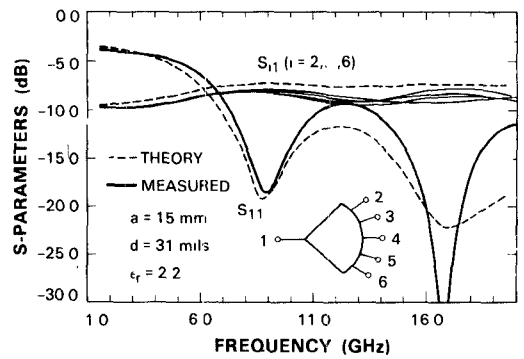

Fig. 6. Measured and calculated performance of a five-way 90° sector power divider.

occurring in (2), (5), and (10) were taken to be 30 each. This value was chosen by noting the convergence of the numerical results in the frequency range of interest. For better convergence at frequencies above 15 GHz, larger values of m and n are needed.

As shown in Figs. 5 and 6 equal power division and good input match are achieved at the frequencies which correspond to the resonances of the $(n,0)$ azimuthal symmetric modes. The port locations in these configurations were determined by dividing the circumferential edge of the sector into N sections ($N = 4$ in Fig. 5 and $N = 5$ in Fig. 6) of equal width. One output port is then positioned at the middle of each of these N sections. Such a choice is primarily influenced by the desire to maintain physical symmetry, which helps in obtaining equal power division.

B. Analysis of 180° Sectorial Circuit

The case of 180° sector shown in Fig. 7 can also be analyzed by using (2) through (10) but with $\alpha = 180°$. However in this case a more accurate analysis is carried out by taking into account the effect of the higher order evanescent modes generated at the junction between the feed port and the sector. This is performed by modeling a small section of the microstrip feed line as a two-dimensional planar component and then using the segmentation procedure [5]. This more accurate approach was implemented and found to produce results very close to those obtained in the previous section (i.e., without the use of segmentation and by combining the four subports into a

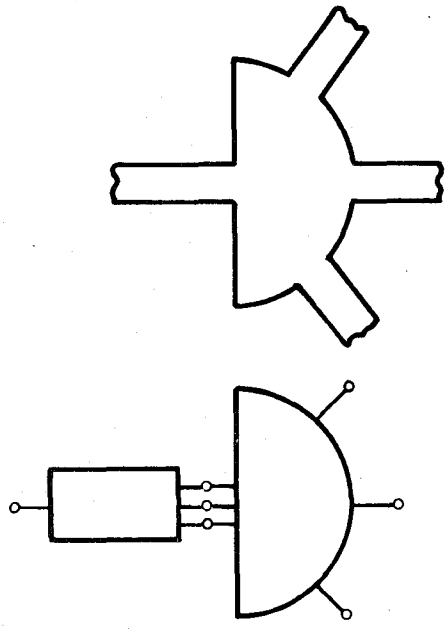

Fig. 7. Analysis of a semicircular power divider circuit.

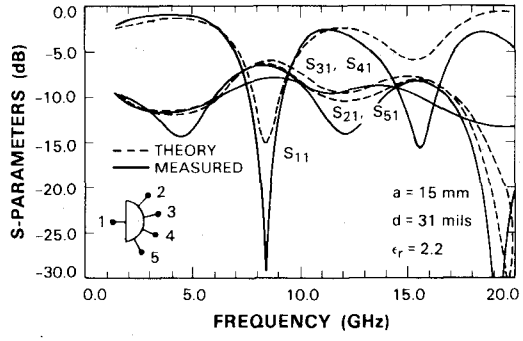

Fig. 8. Measured and calculated scattering parameters of a four-way 180° sector power divider.

single port). Here, again, the values of m and n needed for the convergence of the summations occurring in (2), (5), and (10) were found to be $m = n = 30$, which have been used for the numerical results reported in this paper.

The magnitudes of S_{11}, S_{21}, S_{31}, S_{41}, and S_{51} are plotted as functions of frequency in Fig. 8. Again equal power division was obtained at the resonance frequencies of the (1,0) and (2,0) azimuthal symmetric modes. The asymmetric modes, however, play a more significant role in this case than in the case of 90° sectorial circuits. The presence of these higher order modes disturbs the amplitude balance observed in the 90° sectorial circuits described earlier. Furthermore, the equal power division and good match seem to coincide only over a limited frequency range as shown in Fig. 8.

For the results presented in subsections A and B, the dielectric and conductor losses were incorporated in the same manner as described in [4]. The radiation losses, on the other hand, were not included. It may be noted that for these circuits, which have five or six external ports, the loaded Q factor becomes very small and the radiation loss is expected to be small, even at the resonance.

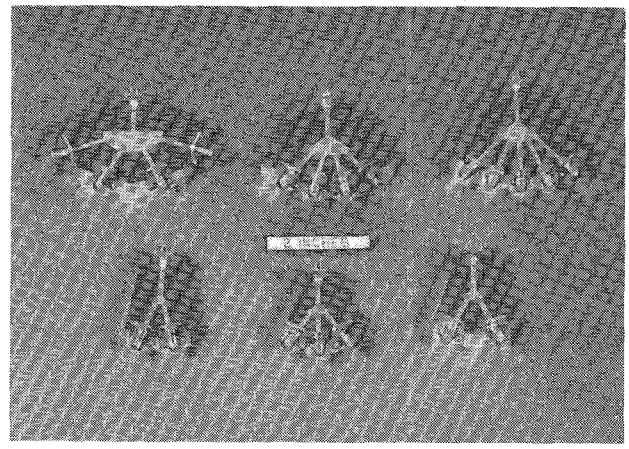

Fig. 9. Photograph of several multiway power divider/combiner sectorial circuits.

III. Experimental Results

In order to verify the accuracy of the method of analysis a number of power divider/combiner circuits have been designed, constructed, and tested. A photograph of these circuits is shown in Fig. 9.

A comparison between the measured and calculated performance of the 90° four-way power divider circuit is shown in Fig. 5. As shown, excellent agreement between the measured and calculated magnitudes of S_{11}, S_{21}, S_{31}, S_{41}, and S_{51} is obtained. The gating feature on the HP 8510 Automatic Network Analyzer (ANA) has been used to remove the effect of the connectors. It is evident from these data that this circuit can be used as a power divider in two different frequency bands. This is because the return loss S_{11} is less than -12 dB in the frequency bands 8–10 GHz and 15–19 GHz. Perfect amplitude balance is obtained both experimentally and theoretically over the lower frequency band. The experimental values of the transmission coefficients were -6.7 dB at the center frequency. In the higher frequency band, the amplitude balance suffers slightly but remains good within ± 0.6 dB. It is believed that the discrepancy between measurement and theory occurring at frequencies above 14 GHz is partly due to the poor convergence of the summations of (2), (5), and (10). An improved convergence was observed when the values of m and n were changed from 20 to 30.

The port-to-port phase balance has been measured and found to be within $\pm 2°$ over the frequency band 8 to 10 GHz. The corresponding theoretical values are within $\pm 0.1°$. The isolation between the output ports varies from -5 to -25 dB over the lower frequency band, whereas the values for the upper frequency band are between -8 and -14 dB, depending upon the port location. These isolation values are obtained without the use of any external resistors. If needed, external resistors can be used to improve the isolation performance of these circuits.

Fig. 6 illustrates a comparison between the measured and calculated scalar characteristics of a five-way 90° power divider. This configuration has the same physical dimensions (i.e., $a = 1.5$ cm and $d = 31$ mils) as the four-

way circuit described in Fig. 5. As in the previous four-way case, the gating feature in the HP 8510 ANA is used to remove the effect of the connectors. Upon inspecting the frequency characteristics of these circuits it becomes apparent that there are two frequency bands of operation. Considering -12 dB to be an acceptable level for the input reflection coefficient S_{11}, the first frequency band is found to be centered around the (1,0) resonant mode and extends from 7.7 to 10.5 GHz. The second frequency band is centered around the resonance frequency of the (2,0) azimuthal symmetric mode and extends from 14.5 GHz to about 19 GHz. Once again discrepancy between theory and measurement starts to appear above 16 GHz.

Finally Fig. 8 shows a comparison between the measured and calculated scalar characteristics of a four-way 180° sector power divider. The amplitude balance in this case is not as good as in the two previous configurations. Furthermore, good impedance matching and equal power division do not occur concurrently at the same frequency. It is believed that this is due to the more significant role played by the higher order modes in this case.

IV. Concluding Remarks

The results reported in this paper indicate that the sectorial planar geometry is a promising configuration for the design of planar multiway power divider–combiner circuits. It may be noted that the experimental and theoretical results shown in this paper are based on the initial ad hoc designs of these circuits. It should be possible to improve the performance of these circuits by selecting optimum values for the various design parameters (such as the widths and locations of the various ports). The two-dimensional analysis reported in Section II is well suited for a computer-aided optimization of these circuits. The agreement between the theoretical and experimental results presented in this paper verifies the validity of the planar two-dimensional circuit analysis approach.

Acknowledgment

The authors are indebted to K. Telley for typing the manuscript and to J. Austin for performing the measurements. Many thanks are also due to A. Dumanian for her help in the computation.

References

[1] A. Fathy and D. Kalokitis, "Analysis and design of a 30-way radial combiner for the *Ku*-band applications," *RCA Rev.*, vol. 47, pp. 487–508, Dec. 1986.

[2] S. J. Foti, R. P. Flam, and W. J. Scharpf, "60-way radial combiner uses no isolators," *Microwaves and RF*, pp. 96–118, July 1984.

[3] A. A. M. Saleh, "Planar electrically symmetric *N*-way hybrid power dividers/combiners," *IEEE Trans. Microwave Theory Tech.*, vol. MTT-28, pp. 555–563, June 1980.

[4] M. D. Abouzahra and K. C. Gupta, "Multiple-port power divider/combiner circuits using circular microstrip disc configurations," *IEEE Trans. Microwave Theory Tech.*, vol. MTT-35, pp. 1296–1302, Dec. 1987.

[5] K. C. Gupta, R. Garg, and R. Chadha, *Computer Aided Design of Microwave Circuits*. Dedham MA: Artech House, 1981, ch. 11.

[6] F. Giannini, R. Sorrentino, and J. Vrba, "Planar circuit analysis of microstrip radial stub," *IEEE Trans. Microwave Theory Tech.*, vol. MTT-32, pp. 1652–1655, Dec. 1984.

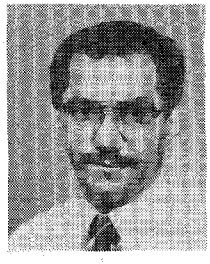

Mohamed D. Abouzahra (S'79–M'85–SM'87) was born in Beirut, Lebanon, on June 15, 1953. He received the B.S. degree (with distinction) in electronics and communications from Cairo University, Cairo, Egypt, in 1976 and the M.S. and Ph.D. degrees in electrical engineering from the University of Colorado, Boulder, in 1978 and 1984, respectively.

From 1979 to 1984 he worked as a research and teaching assistant at the University of Colorado, Boulder. Since 1984 he has been a member of the Countermeasures Technology group at the Massachusetts Institute of Technology, Lincoln Laboratory. He has worked on microstrip line discontinuities, wide-band dielectric directional couplers, and dielectric image lines. He is currently interested in the computer-aided design of microwave and millimeter-wave wide-band planar circuits, and in the development of wide-band automated measurement schemes for characterizing composite materials.

Dr. Abouzahra has published over 20 research papers and holds one patent in the microwave area. He is also a coauthor of a chapter in the forthcoming book *Numerical Techniques for Microwave and Millimeter Wave Passive Structures* (John Wiley).

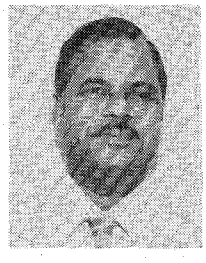

Kuldip C. Gupta (M'62–SM'74–F'88) received the B.S. and M.S. degrees in electrical communication engineering from Indian Institute of Science, Bangalore, India, in 1961 and 1962, respectively, and the Ph.D. degree from Birla Institute of Technology and Science, Pilani, India, in 1969.

He has been at the University of Colorado since 1983, initially as a Visiting Professor and later as a full Professor. Earlier he had a long stay (since 1969) at Indian Institute of Technology, Kanpur (India), where he has been a full Professor in Electrical Engineering since 1975. On leave form IITK, he has been a Visiting Professor at the University of Waterloo, Canada; at Ecole Polytechnique Federale de Lausanne, Switzerland; at the Technical University of Denmark (Lyngby); at the Eidgenossische Technische Hochschule, Zurich; and at the University of Kansas, Lawrence. From 1971 to 1979 he was the Coordinator for the Phase Array Radar Group of the Advanced Center for Electronics Systems at the Indian Institute of Technology. His current research interests are in the area of computer-aided design techniques for microwave/millimeter-wave integrated circuits and integrated antennas.

Dr. Gupta is the author or coauthor of four books: *Microwave Integrated Circuits* (Wiley Eastern 1974, Halsted Press of John Wiley 1974), *Microstrip Lines and Slotlines* (Artech House 1979), *Microwave* (Wiley Eastern 1979, Halsted Press of John Wiley 1980, Editorial Limusa Mexico 1983), and *CAD of Microwave Circuits* (Artech House 1981, Chinese Scientific Press 1986). Also, he has contributed chapters to the forthcoming *Handbook of Microstrip Antennas* (Peter Peregrinus) and *Handbook of Microwave and Optical Components* (John Wiley). Dr. Gupta has published over 100 research papers and holds one patent in the microwave area. He is a Fellow of the Institution of Electronics and Telecommunication Engineers (India). He is on the MTT-S Technical Committee on CAD, on the Editorial Board for the MTT-S Transactions, and on the Technical Program Committee for MTT-S International Symposia. He served as a Guest Editor of the 1988 Special Issue of MTT Transactions on Computer-Aided Design.